


Optical Energy-Difference Conservation in a Synthetic Anti-PT-Symmetric System

Sebae Park,^{*} Dongjin Lee,^{*} Kyungdeuk Park, and Heedeuk Shin[†]

Department of Physics, Pohang University of Science and Technology (POSTECH), Pohang 37673, South Korea

Youngsun Choi and Jae Woong Yoon

Department of Physics, Hanyang University, Seoul 04763, South Korea

 (Received 4 April 2021; accepted 12 July 2021; published 17 August 2021)

Anti-parity-time (APT) symmetry is associated with various effects beyond the fundamental limitations implied in the standard Hermitian-Hamiltonian dynamics. Here, we create an optical APT-symmetric system in a synthetic frequency domain using a conventional fiber without intrinsic gain or loss and experimentally reveal photonic APT-symmetric effects, including energy-difference conservation and synchronized power oscillation, which have not yet been confirmed experimentally in the optical domain. The optical fiber-based APT-symmetric system has a long interaction length because of its negligible loss, and the APT-symmetric Hamiltonian is precisely tunable with optical pumping density and phase mismatch. On this basis, we observe the phase transition at exceptional points, energy-difference conservation, and synchronized power oscillation. Our results provide a robust theoretical and experimental framework connecting the emerging non-Hermitian physics with technologically important nonlinear fiber-optic interactions.

DOI: [10.1103/PhysRevLett.127.083601](https://doi.org/10.1103/PhysRevLett.127.083601)

Recent developments in non-Hermitian physics have opened up intriguing possibilities for novel wave properties by intentionally engaging internal physical activities with environmental interventions. For example, carefully designed gain and loss in connection with interstate coupling strength have produced numerous anomalous effects associated with the parity-time (PT) symmetry [1–7] and exceptional-point (EP) singularity [8], studying the class of Hamiltonian that commutes or anticommutes with PT operation, referred to as the PT or anti-PT-symmetric system, respectively [3,9]. Such effects include spontaneous symmetry-breaking phase transitions [1–3,5,10,11], autotuned wireless power transfer [12], unidirectional diffraction [13–15], refractionless media [9], and time-asymmetric topological operations [16,17]. These non-Hermitian phenomena have no counterpart among conventional closed-system properties. Studying non-Hermitian systems in conceptually far-reaching open-system domains is of great interest to create powerful theoretical tools and practical technologies beyond the inherent limitations in previously established Hermitian-system approaches.

Beyond the geometric dimension, it is possible to explore physics in new dimensions such as frequency, time, and orbital angular momentum, which are referred to as synthetic dimensions [18]. Non-Hermitian systems using nonlinear wave-mixing processes in the synthetic frequency domain provide efficient experimental flexibility for configuring desired coherent environmental interventions [19–21]. Recently, anti-PT (APT) symmetry through

four-wave-mixing (FWM) has been realized in cold atoms [19] and optical fibers [21], resulting in APT-symmetric phase transition and non-Hermitian dynamics around the EP.

Most of these experiments were performed with incompletely balanced gain and loss in an effective PT-symmetric system or loss-dominant quasi-PT-symmetric system [4]. Energy-difference conservation (EDC) in APT symmetry is in contrast to the standard Hermitian dynamics' net-energy conservation and the cross-conjugate product conservation of the PT-symmetric dynamics [22], requiring a perfectly balanced gain and loss. EDC has been implemented only in electrical circuits [22], but there have been no reports of EDC in the optical domain because of various fabrication difficulties for the precise control of optical gain and loss. The APT-symmetric EDC may provide new methods for optical manipulation, including antiadiabatic topological time asymmetry [16,17], EP-related unidirectionality [3,13,14], and diverging parametric sensitivity [23,24].

In this Letter, we show that the anti-PT-symmetric Hamiltonian naturally arises in the degenerate FWM process and consequently follows a pseudo-Hermitian conservation law, i.e., the optical energy-difference conservation. We develop an APT-symmetric Hamiltonian theory of a third-order nonlinear optical system that does not involve any explicit material gain and loss mechanisms, and we observe the spontaneous symmetry-breaking phase transition and synchronized power oscillation behaviors. The proposed APT-symmetric system uses a fiber-optic platform, taking advantage of the long interaction length,

practicality, relative ease of system construction, and negligible optical gain and loss [25,26]. Because of this gainless-lossless system, we experimentally observe the optical EDC behaviors for the first time, in excellent agreement with the theory regarding the key physical aspects, including energy-spectral properties and dynamic responses.

FWM is a third-order nonlinear process inducing a coupling between different frequency modes [27]. The frequencies of the signal and idler are determined as $2\nu_p - \nu_s = \nu_i$, where ν_p , ν_s , and ν_i are the pump, signal, and idler frequencies, respectively. In a lossless medium under a high-power nondepleted pump, weak seed signal and generated idler waves can be described as two coupled states in a binary system. The signal-field amplitude (A_s) and idler-conjugate-field amplitude (A_i^*) obey the Schrödinger-like coupled equation [1,2,4]

$$i\hbar c \frac{\partial}{\partial z} \begin{pmatrix} A_s \\ A_i^* \end{pmatrix} = H_{\text{APT}} \begin{pmatrix} A_s \\ A_i^* \end{pmatrix}, \quad (1)$$

where the effective Hamiltonian is given by (see Supplemental Material, Sec. I [28])

$$H_{\text{APT}} = \begin{pmatrix} -\epsilon & i\kappa \\ i\kappa & \epsilon \end{pmatrix} = \hbar c \begin{pmatrix} -\Delta k/2 - \gamma P_p & i\gamma P_p \\ i\gamma P_p & \Delta k/2 + \gamma P_p \end{pmatrix}. \quad (2)$$

2ϵ , κ , γ , and P_p represent the energy difference, coupling coefficient between two modes, third-order nonlinear coefficient, and pump power, respectively. $\Delta k = k_s + k_i - 2k_p$ is the wave vector mismatch, where k_s , k_i , and k_p correspond to the wave vector of the signal, idler, and pump fields, respectively. Note that this effective Hamiltonian satisfies the APT symmetry, i.e., $(PT)H_{\text{APT}}(PT)^{-1} = -H_{\text{APT}}$, denoting a simple sign change of the Hamiltonian under PT reversal (see Supplemental Material, Sec. I [28]). The pure imaginary coupling constant indicates gain or loss [29]. Through proper gauge transformation, we obtain an identical and pure-imaginary coupling constant, which is in contrast to the real coupling constant (i.e., conjugated) in a Hermitian system. As the pump power is much larger than that of the signal and idler, we can consider the pump an environment for the system of interest.

In the proposed synthetic APT-symmetric system, two frequency modes in a single-mode waveguide couple to each other with coupling coefficient $i\kappa$. The eigenvalue of the system is given by

$$\xi_{\pm} = \pm\xi = \pm\sqrt{\epsilon^2 - \kappa^2} = \pm\hbar c \frac{\Delta k}{2} \sqrt{1 + \frac{4\gamma P_p}{\Delta k}}. \quad (3)$$

The eigenvalue changes from a real value to an imaginary value when the sign inside the root varies from positive to

negative, indicating the spontaneous symmetry-breaking phase transition. In APT-symmetric systems, having a pure imaginary eigenvalue is identical to the case where the corresponding eigenstate is invariant under the PT operation (see Supplemental Material, Sec. II [28]). Thus, the transition from the real to the pure imaginary eigenspectra corresponds to the phase transition from the broken PT-symmetry phase to the exact PT-symmetry phase [11]. In the anomalous dispersion regime ($\Delta k < 0$), the symmetry-breaking phase transition can be readily obtained by sweeping the pump power. The point where the phase transition occurs ($\Delta k[\Delta k + 4\gamma P_p] = 0$) is referred to as an exceptional point (EP). In addition, our APT-symmetric systems have pseudo-Hermiticity, such that $H_{\text{APT}}^{\dagger} = \sigma_z H_{\text{APT}} \sigma_z$, where σ_z is the Pauli matrix [22,33]. Therefore, the energy difference between the signal and idler modes is conserved along the propagation direction (z axis), corresponding to the Schrödinger equation time axis.

When the signal field is seeded, a normal-mode solution of Eq. (1) is given by

$$|A_i^*|^2 = |A_s|^2 - C = \frac{C\kappa^2}{\xi^2} \sin^2 \frac{\xi z}{\hbar c} = \frac{C \cdot \kappa^2}{\epsilon^2 - \kappa^2} \sin^2 \frac{z\sqrt{\epsilon^2 - \kappa^2}}{\hbar c}. \quad (4)$$

C is the input seed power. The idler intensity $|A_i^*|^2$ dependence on propagation distance z drastically changes as eigenvalue ξ changes its value from a real to a pure imaginary number at the EP, i.e., from a simple sinusoidal oscillation for purely real ξ in the broken PT-symmetry phase, a quadratic dependence $(\hbar c)^{-2}\kappa^2 z^2$ for $\xi = 0$ at the EP, and to an exponential dependence for purely imaginary ξ in the exact PT-symmetry phase.

The power difference remains constant at the input seed power, regardless of the z value, i.e., $|A_s(z)|^2 - |A_i^*(z)|^2 = C$, which is in contrast to the conventional Hermitian-Hamiltonian system. Unlike Hermitian systems where the powers of two coupled channels oscillate with opposite phase, i.e., $|A_s(z)|^2 + |A_i^*(z)|^2 = C$, the powers of the two channels in the APT-symmetric system oscillate synchronously with the same phase in the broken PT-symmetry phase (having real eigenvalues). In a more fundamental consideration, this intensity-difference-conserving property originates from the pseudo-Hermiticity implied in the APT symmetry, as explained in Ref. [22].

Our experimental schematic is shown in Fig. 1. A dispersion-shifted fiber (DSF) is the FWM medium that produces our desired APT-symmetric effects. We investigate the APT dynamic responses in a parameter space defined by pump power and frequency detuning. The measured dispersion properties [34] of the DSF are a zero group-velocity-dispersion (GVD) wavelength (λ_0) of 1533.5 nm and a dispersion slope of 71.6 s/m³, and the length of the DSF is 2 km. The frequency of the pump laser

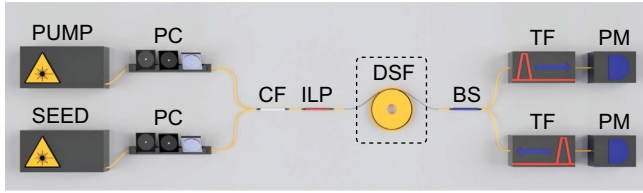


FIG. 1. Experimental setup of the proposed system. PUMP, pump laser; SEED, seed laser; PC, polarization controller; CF, combining filter; DSF, dispersion-shifted fiber; ILP, in-line polarizer; BS, beam splitter; TF, tunable filter; PM, power meter.

is fixed at 192.2 THz (1559.79 nm), which is in the anomalous dispersion region ($\lambda_p > \lambda_0$), resulting in negative wave vector mismatch ($\Delta k < 0$).

Frequency detuning ($\Delta\nu$) of the seed laser from the pump frequency varies from 0.2 to 0.4 THz, where its peak power is approximately 1 μ W. The pump peak power ranges from near 0 to 1.8 W. We restrict the pump peak power to less than 1.8 W to avoid unfavorable nonlinear effects, including pump depletion resulting from the cascaded FWM (see Supplemental Material, Sec. III [28]). The synchronized pump and seed lasers' temporal width and repetition rates are 3 ns and 10 MHz, respectively. Pump and seed pulses are mixed with a combining filter. We match the pump and seed beam polarization states using polarization controllers and an in-line polarizer. After a beam splitter, one tunable filter is set to the signal (seeded) frequency, and the other to the corresponding idler (generated) frequency. The measured intensity values are calibrated with our setup net efficiency, yielding the estimated peak intensities at the output port of the DSF. The noise level in our detection method is on the order of nanowatts.

Figure 2(a) shows the measurement results for the output signal and idler pulse peak powers in $\Delta\nu - P_p$ parameter space, in comparison with the theoretical calculations given in Fig. 2(b). Above the noise level (nanowatts), they are in excellent agreement in all desired aspects, including power oscillation, quadratic growth, and exponential amplification with respect to the EP loci indicated by red curves. The domain is different from that of a Riemann surface. The Hamiltonian satisfies the APT symmetry in the whole parameter space ($\Delta\nu$ and P_p). Note that the parameters in the APT Hamiltonian are constant along the time or propagation direction.

In addition, the measured signal and idler powers evolve in a similar fashion with increasing negative wave vector mismatch at fixed pump power. The wave vector mismatch Δk is controlled by varying the pump wavelength, zero GVD wavelength, and frequency detuning $\Delta\nu$ between the pump and seed lasers (see Supplemental Material, Sec. IV [28]). As expected, the idler power shows oscillating behavior under the conditions of $\Delta\nu > \Delta\nu_{EP}$ and $P_p < P_{p,EP}$ and amplification under $\Delta\nu < \Delta\nu_{EP}$ and $P_p > P_{p,EP}$, where $\Delta\nu_{EP}$ is the frequency detuning at EP. The results

show that characteristic non-Hermitian properties are inherent in the FWM effects, which are key processes for parametric amplification [35].

Figure 3 shows the intersection of Fig. 2 versus the pump power for various frequency detuning $\Delta\nu$ values. Signal (blue) and generated idler (red) powers for $\Delta\nu = 0.27$, 0.30, and 0.33 THz are indicated in Figs. 3(a), 3(b), and 3(c), respectively. The areas above the EP pump power $P_{p,EP}$ are shaded in gray. The solid curves show that the theoretical calculation matches well with the experimental data, using the measured input pump and signal powers, the estimated phase mismatch (Δk), and an extracted nonlinear coefficient (γ). γ is extracted as 1.51 $\text{W}^{-1} \text{km}^{-1}$ by fitting Eq. (4) to the data in Fig. 3 and used for Figs. 2 and 3. The idler power does not follow the theoretical curves for the sharp minima; this may be due to imperfections in the experiments, such as nonuniform DSF. Assuming a non-uniform DSF, the theoretical calculations show that the mismatch between the experimental data and the theory decreases. See Supplemental Material, Sec. V, for the full comparison results [28]. Note that the oscillation below $P_{p,EP}$ and amplification above $P_{p,EP}$ represent the characteristic responses associated with the spontaneous symmetry-breaking phase transition. Above $P_{p,EP}$, both the signal and idler powers are amplified, even though the system has both plus and minus pure imaginary eigenvalues related to the nonlinear gain or loss. This is because the eigenstate corresponding to the gain in Eq. (1) is invariant under PT operation, meaning that the eigenstate has an equal magnitude for signal and idler fields. Therefore, the simultaneous amplification in the signal and idler powers confirms the equivalence relationship between the pure imaginary eigenspectra and the exact PT-symmetry phase.

The spontaneous symmetry-breaking phase transition is more obvious if the signal and idler powers are normalized by their sum, as shown in Figs. 3(d), 3(e), and 3(f) for $\Delta\nu = [0.27, 0.30, 0.33]$ THz, respectively. As the intensity difference between the signal and idler powers is conserved, the signal and idler power amplification above $P_{p,EP}$ leads to the convergence of the power ratio between them to 1. Therefore, the normalized powers oscillate below $P_{p,EP}$ and converge to 1/2 above $P_{p,EP}$. In addition, we repeat the measurements for the negative frequency detuning of the seed laser from 0.2 to 0.4 THz, and the results are identical to results for positive frequency detuning, as the sign of $\Delta\nu$ does not change the wave vector mismatch. See Supplemental Material, Sec. VI and Video S1 [28].

Figures 3(g)–3(i) show the experimental eigenvalues inferred from the measurement data in Figs. 3(a)–3(c). See Supplemental Material, Sec. VII [28], for details of the eigenvalue-estimation method. The inferred eigenvalue spectra show the real and pure imaginary eigenspectra below and above $P_{p,EP}$, respectively. In the low-pump-power range, the real eigenvalue does not match the

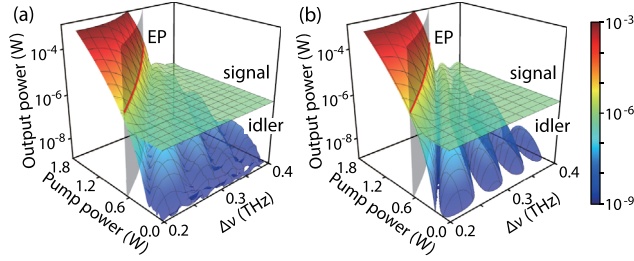


FIG. 2. Phase transition between oscillation and amplification in the $\Delta\nu$ and P_p parameter space. The power of the signal and generated idler beams on a log scale are presented in the $\Delta\nu$ and P_p parameter space. (a) is the experimental result, and (b) is the theoretical calculations [note Eq. (4)]. The red line is the calculated power of the signal light at the EP pump power. The transparent gray surface is the guided surface of the EP in the parameter space.

theoretical value, as the measurement of the idler output power is not accurate below the noise level ($\sim 10^{-9}$ W), as shown in Figs. 3(a)–3(c). As seen in Fig. 3, we experimentally confirm the symmetry-breaking phase transition of our photonic APT-symmetric system.

We further investigate the pseudo-Hermiticity effects in our fiber-optic platform. The intensity difference between two basis states [$\langle \psi(z) | \sigma_z | \psi(z) \rangle$] is conserved in the z axis, indicating no net energy exchange between the two basis states [22,33]. See Supplemental Material, Sec. VIII [28]. In this analysis, we explore this unique pseudo-Hermiticity effect by varying the propagation length. In Eq. (2), the APT symmetry is preserved if each individual channel has the same amount of gain or loss; i.e., adding the same pure imaginary number to both diagonal components of the Hamiltonian does not affect the APT-symmetric physical condition of a system. However, as unbalanced gain and loss lead to a change in the energy difference, it was quite challenging to experimentally confirm the APT-symmetric energy-difference conservation effect in the optical domain [19,36]. Our fiber-optic APT-symmetric system takes great advantage of long interaction time, i.e., long propagation length and virtually lossless characteristic of commercially available fiber-optic cables, which may enable observation of this unique pseudo-Hermitian effect in the optics realm.

In this observation, we use the cutback method, where the length of the DSF sample varies from 2 to 1 km, with a step length of 100 m. We prepared another DSF sample with similar dispersion properties: a zero GVD wavelength of 1527.41 nm, dispersion slope of 72.6 s/m³, and extracted nonlinear coefficient γ of 1.46 W⁻¹ km⁻¹ which is comparable with the reported values [37]. We measure the optical powers of the final signal and idler states and monitor the change in their difference. Figures 4(a), 4(b), and 4(c) show the experimental and theoretical results for various frequency detunings at 0.10, 0.15, and 0.20 THz, respectively, when the pump power is fixed at

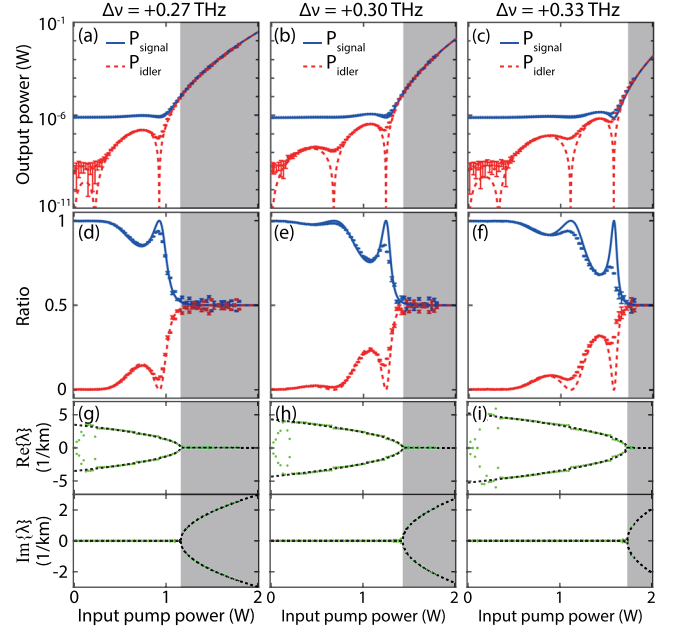


FIG. 3. Phase transition behaviors versus pump power. (a)–(c) The seeded signal and generated idler powers on a log scale are plotted against the input pump power. The background is shaded gray above the EP pump power. The lines are the calculated signal and idler powers. (d)–(f) The signal and idler powers normalized by their sum in (a)–(c), respectively. (g)–(i) The extracted eigenvalues from the data in (a)–(c) on a linear scale. In (a),(d),(g), (b),(e),(h), and (c),(f),(i), the detuning between the pump and seed lasers is set to 0.27, 0.30, and 0.33 THz, respectively.

$P_p = 0.47$ W. As $P_{p,EP}$'s for these detunings are [0.22, 0.47, 0.83] W, respectively, the three cases represent the conditions of above, right at, and below the EP, respectively. The signal and idler powers undergo different dynamics for these exemplary cases, i.e., exponential growth for Fig. 4(a) above the EP, quadratic growth for Fig. 4(b) at the EP, and periodic oscillation for Fig. 4(c) below the EP. For all of these cases, the measured power difference is conserved at the same value (~ 1 μ W). The points and error bars of the signal and idler powers are the mean and standard deviation values out of ten repeated measurements. The points and error bars of the difference are calculated assuming Gaussian statistics for the difference between the means and root-sum-square values of the standard deviations. See Supplemental Material, Video S2 [28], for fine-tuned analysis of Fig. 4. Importantly, this is the first observation of the unique optical EDC, to the best of our knowledge.

In addition, we repeat the measurements with different detunings and pump powers to investigate the APT-symmetric power oscillating behaviors below the EP threshold. Figures 4(d), 4(e), and 4(f) show the seeded signal (blue) and generated idler (red) powers for $\Delta\nu = [0.29, 0.30, 0.31]$ THz, respectively, at a fixed pump

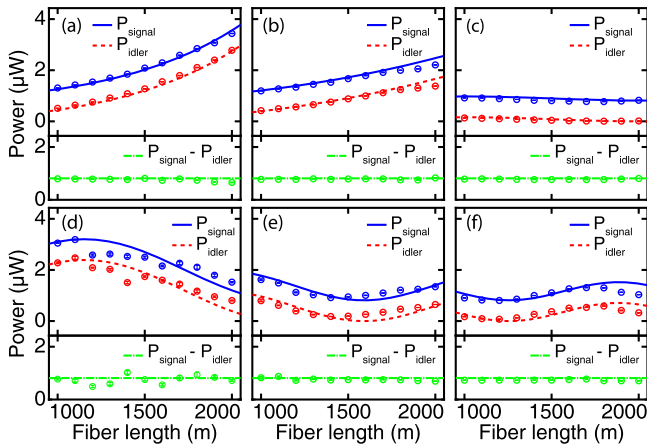


FIG. 4. Energy-difference conservation and bounded oscillation. The signal (blue dots and lines) and idler (red dots and lines) output powers and the difference between them (green dots and lines) are represented on a linear scale for detunings of (a) 0.10, (b) 0.15, and (c) 0.20 THz at a fixed pump power of 0.47 W, showing EDC above, right at, and below the EP, and for detunings of (d) 0.29, (e) 0.30, and (f) 0.31 THz at a fixed pump power of 1.6 W, showing bounded oscillation and EDC below the EP. The lines represent theoretical predictions.

power of $P_p = 1.6$ W. The corresponding EP pump powers are $P_{p,EP} = [1.74, 1.88, 1.99]$ W, respectively. The measured signal and idler powers oscillate in unison, as seen in Figs. 4(d)–4(f). As the detuning increases, the $|\epsilon|$ increases. Then, both the amplitude and period of the APT-symmetric power oscillation decrease, as predicted in Eq. (4). In addition, the power difference between the signal and idler powers is persistently conserved. See Supplemental Material, Video S3 [28], for fine-tuned analysis of Fig. 4.

In conclusion, we have established a synthetic non-Hermitian optical system based on FWM nonlinearity in a lossless-gainless fiber-optic platform. In addition to demonstrating the anomalous APT-symmetric effects, we expect antiadiabatic topological time asymmetry in our platform (see Supplemental Material, Sec. IX [28], for how to realize topological operation in our platform). The properties with a lossless-gainless APT-symmetric system are highly favorable for further development in various technology areas, such as telecommunications, sensing, and areas in which most previous non-Hermitian photonic systems are limited. Furthermore, the single-mode fiber and FWM mechanism used in this system have been intensively studied to generate photon pairs or squeezed states of light as quantum light sources [25,26,38,39]. Therefore, we expect to combine the synthetic non-Hermitian systems and quantum information systems in the future. Finally, we believe that our result provides a robust and efficient experimental platform for a further in-depth study on open-system APT dynamics as well as concomitant device

applications in practice and will enable of future interdisciplinary study.

The work was supported by the National Research Foundation of Korea (NRF-2019M3E4A1079780), Institute for Information and communications Technology Promotion (IITP) grant funded by the Korea government (MSIT) (No. 2020-0-00947), and Korea Institute of Science and Technology's Open Research Program (2E30620-20-052). S. P. was supported by the Global Ph.D. Fellowship Program of the National Research Foundation of Korea (NRF-2019H1A2A1074326). J. W. Y. acknowledges support through the Leader Researcher Program (NRF-2019R1A3B2068083), and Y. C. was funded by the Presidential Post-Doc Fellowship Program of the National Research Foundation of Korea (NRF-2017R1A6A3A04011896).

*These authors contributed equally to this work.

†heedeukshin@postech.ac.kr

- [1] A. Guo, G. J. Salamo, D. Duchesne, R. Morandotti, M. Volatier-Ravat, V. Aimez, G. A. Siviloglou, and D. N. Christodoulides, *Phys. Rev. Lett.* **103**, 093902 (2009).
- [2] C. E. Rüter, K. G. Makris, R. El-Ganainy, D. N. Christodoulides, M. Segev, and D. Kip, *Nat. Phys.* **6**, 192 (2010).
- [3] B. Peng, Ş. K. Özdemir, F. Lei, F. Monifi, M. Gianfreda, G. L. Long, S. Fan, F. Nori, C. M. Bender, and L. Yang, *Nat. Phys.* **10**, 394 (2014).
- [4] L. Feng, R. El-Ganainy, and L. Ge, *Nat. Photonics* **11**, 752 (2017).
- [5] Y. Wu, W. Liu, J. Geng, X. Song, X. Ye, C.-K. Duan, X. Rong, and J. Du, *Science* **364**, 878 (2019).
- [6] J. Christensen, M. Willatzen, V. R. Velasco, and M.-H. Lu, *Phys. Rev. Lett.* **116**, 207601 (2016).
- [7] B. Qi, H.-Z. Chen, L. Ge, P. Berini, and R.-M. Ma, *Adv. Opt. Mater.* **7**, 1900694 (2019).
- [8] W. D. Heiss, *J. Phys. A* **45**, 444016 (2012).
- [9] P. Peng, W. Cao, C. Shen, W. Qu, J. Wen, L. Jiang, and Y. Xiao, *Nat. Phys.* **12**, 1139 (2016).
- [10] C. M. Bender and S. Boettcher, *Phys. Rev. Lett.* **80**, 5243 (1998).
- [11] C. M. Bender, *Rep. Prog. Phys.* **70**, 947 (2007).
- [12] S. Assaworarrat, X. Yu, and S. Fan, *Nature (London)* **546**, 387 (2017).
- [13] Z. Lin, H. Ramezani, T. Eichelkraut, T. Kottos, H. Cao, and D. N. Christodoulides, *Phys. Rev. Lett.* **106**, 213901 (2011).
- [14] L. Feng, Y.-L. Xu, W. S. Fegadolli, M.-H. Lu, J. E. B. Oliveira, V. R. Almeida, Y.-F. Chen, and A. Scherer, *Nat. Mater.* **12**, 108 (2013).
- [15] P. Miao, Z. Zhang, J. Sun, W. Walasik, S. Longhi, N. M. Litchinitser, and L. Feng, *Science* **353**, 464 (2016).
- [16] J. W. Yoon, Y. Choi, C. Hahn, G. Kim, S. H. Song, K.-Y. Yang, J. Y. Lee, Y. Kim, C. S. Lee, J. K. Shin, H.-S. Lee, and P. Berini, *Nature (London)* **562**, 86 (2018).
- [17] X.-L. Zhang, T. Jiang, and C. T. Chan, *Light Sci. Appl.* **8**, 88 (2019).
- [18] L. Yuan, Q. Lin, M. Xiao, and S. Fan, *Optica* **5**, 1396 (2018).

- [19] Y. Jiang, Y. Mei, Y. Zuo, Y. Zhai, J. Li, J. Wen, and S. Du, *Phys. Rev. Lett.* **123**, 193604 (2019).
- [20] F. Zhang, Y. Feng, X. Chen, L. Ge, and W. Wan, *Phys. Rev. Lett.* **124**, 053901 (2020).
- [21] A. Bergman, R. Duggan, K. Sharma, M. Tur, A. Zadok, and A. Alú, *Nat. Commun.* **12**, 486 (2021).
- [22] Y. Choi, C. Hahn, J. W. Yoon, and S. H. Song, *Nat. Commun.* **9**, 2182 (2018).
- [23] W. Chen, Ş. K. Özdemir, G. Zhao, J. Wiersig, and L. Yang, *Nature (London)* **548**, 192 (2017).
- [24] H. Hodaie, A. U. Hassan, S. Wittek, H. Garcia-Gracia, R. El-Ganainy, D. N. Christodoulides, and M. Khajavikhan, *Nature (London)* **548**, 187 (2017).
- [25] M. Fiorentino, P. L. Voss, J. E. Sharping, and P. Kumar, *IEEE Photonics Technol. Lett.* **14**, 983 (2002).
- [26] K. Park, D. Lee, Y. S. Ihn, Y.-H. Kim, and H. Shin, *New J. Phys.* **20**, 103004 (2018).
- [27] R. W. Boyd, *Nonlinear Optics* (Academic, New York, 2020).
- [28] See Supplemental Material <http://link.aps.org/supplemental/10.1103/PhysRevLett.127.083601> for a detailed description of the theoretical derivation, experimental consideration, data representation, and a proposal for topological operation, which contains Refs. [11,16,17,29–32].
- [29] S. Zhang, Z. Ye, Y. Wang, Y. Park, G. Bartal, M. Mrejen, X. Yin, and X. Zhang, *Phys. Rev. Lett.* **109**, 193902 (2012).
- [30] M. Eiselt, R. M. Jopson, and R. H. Stolen, *J. Lightwave Technol.* **15**, 135 (1997).
- [31] A. Martinez, M. Dubov, I. Khrushchev, and I. Bennion, *Electron. Lett.* **40**, 1170 (2004).
- [32] R. J. Williams, C. Voigtlander, G. D. Marshall, A. Tinnermann, S. Nolte, M. J. Steel, and M. J. Withford, *Opt. Lett.* **36**, 2988 (2011).
- [33] A. Mostafazadeh, *Int. J. Geom. Methods Mod. Phys.* **07**, 1191 (2010).
- [34] S. J. Jung, J. Y. Lee, and D. Y. Kim, *Opt. Express* **14**, 35 (2006).
- [35] G. P. Agrawal, *Nonlinear Fiber Optics* (Springer, New York, 2000).
- [36] H. Fan, J. Chen, Z. Zhao, J. Wen, and Y.-P. Huang, *ACS Photonics* **7**, 3035 (2020).
- [37] K. S. Kim, R. H. Stolen, W. A. Reed, and K. W. Quoi, *Opt. Lett.* **19**, 257 (1994).
- [38] S. Scheel and A. Szameit, *Europhys. Lett.* **122**, 34001 (2018).
- [39] J. E. Sharping, M. Fiorentino, and P. Kumar, *Opt. Lett.* **26**, 367 (2001).